

Diosgenin Inhibits Prostate Cancer Progression by Inducing UHRF1 Protein Degradation

Rong Tang¹, Yuchong Peng¹, Liuyang Ding¹, Youhong Liu², Linglong Yin¹, Yongming Fu¹, Tanggang Deng¹, and Xiong Li¹

¹The First Affiliated Hospital of Guangdong Pharmaceutical University

²Central South University

May 12, 2022

Abstract

Background and Purpose: Aberrant overexpression of UHRF1 has been reported in several cancer types and UHRF1 is regarded as a novel drug target for cancer therapy. However, no UHRF1-targeted specific small compound inhibitor has been registered in clinical trials. **Experimental Approach:** Network pharmacology together with molecular docking were used to screened a natural molecule bank for PCa treatment. The expression of related protein or mRNA were evaluated by WB and RT-PCR. The ubiquitination levels were assessed by WB. CCK8 assess was used to measuring cells viability. Additionally, PCa cells cycle were analysed by cytofluorimetry, genomic DNA methylation was assessed by Dot blot analysis. Cellular senescence was assessed by Senescence-Associated β -Galactosidase Staining Kit. DU145 cell xenograft models were used to assess the in vivo effect of DSG inhibition. **Key Results:** Identified DSG as a new natural compound specifically targeting UHRF1 protein degradation through the ubiquitin-proteasome pathway, DSG-induced UHRF1 protein degradation reduced the level of genomic DNA methylation, and re-activated the expression of such TSGs as p21, p16 and LXN, thereby resulted in cell cycle arrest, cell senescence and reduced DU145 xenograft tumor growth. Altogether, clarified DSG anticancer mechanism as an epigenetic regulatory drug for the treatment of PCa. **Conclusions and Implications:** Our results first time identified DSG which extract from natural plants specifically targeting UHRF1 protein. This vpresent study provided a promising strategy to discover new molecule-targeted drug from natural compounds. **KEYWORDS:** Traditional Chinese Medicine; Prostate cancer; Diosgenin; DNA methylation; Tumor suppressor genes;

INTRODUCTION

Prostate cancer (PCa) is one of the most incident and prevalent cancers in men worldwide and a leading cause of cancer-related morbidity and mortality (Siegel, et al., 2021). Current therapeutic strategies for localised PCa include androgen deprivation therapy (ADT), surgery, radio-, chemotherapy and others. ADT is the first line standard treatment of patients with newly diagnosed metastatic PCa, patients initially well respond to ADT, but drug resistance shortly develops and the disease continues to progress to castration refractory PCa (CRPC) (Litwin&Tan, 2017, Watson, et al., 2015, Gao, et al., 2010). Therefore, it is urgently needed to identify new diagnostic and therapeutic targets when the diseases develop to CRPC.

Epigenetic modifications, including aberrant DNA methylation and histone modifications contribute to the initiation and progression of PCa (Ruggero, et al., 2018, Arita, et al., 2012, Bert, et al., 2013). Ubiquitin-like PHD and RING finger domain-containing protein 1 (UHRF1) is an important epigenetic regulator that contains multiple functional domains, including the N-terminal ubiquitin-like domain (UBL), tandem Tudor domain (TTD), plant homeodomain (PHD), SET- and Ring finger-associated (SRA) and really interesting new gene (RING) domains, which are responsible for maintaining the fidelity of DNA methylation patterns during DNA replication (Arita, et al., 2012, Patnaik, et al., 2018). UHRF1 is a typical oncogene aberrantly overexpressed in a number of cancer types. In addition to gene amplification, the aberration of post

translational modifications (PTMs) of UHRF1 such as phosphorylation and ubiquitination results in the dysregulation of protein degradation (Yang, et al., 2017, Chen, et al., 2013). UHRF1 overexpression suppresses the transcription of a panel of tumor suppressor genes (TSGs) by regulating DNA methylation. Reversely, inhibition of UHRF1 re-activates TSGs and induces cell cycle arrest and cellular senescence (Beck, et al., 2018, Jung, et al., 2017, Pérez-Mancera, et al., 2014). Therefore, UHRF1 is a potential therapeutic target for PCa. A lot of efforts have been made to develop novel UHRF1-targeted drugs by academics and industries, but no UHRF1-specific small compound inhibitor has been registered in the current clinical trials.

Traditional Chinese medicine (TCM) is an ancient medicine, which is based on more than 3500 years of Chinese medical practice (Su, et al., 2020). TCM has received more and more attention in recent years, and Chinese herbal extracts have immense potential for cancer treatment, and are important resources for new drug discovery (Hsieh, et al., 2014, Zhang, L., et al., 2020). Clinical studies have shown that TCM not only alleviates the symptoms of cancer patients and improves their quality of life but also diminishes adverse reactions and complications caused by chemotherapy, radiotherapy, or targeted-therapy (Duan&Wang, 2002). TCM formulas has been widely used as the complementary and alternative medicine for PCa, and many herbal extracts have demonstrated the anti-cancer efficacy in the *in vitro* models (Zhang, et al., 2019). Monomers extracted from Chinese herbal medicine, such as artemisinin, ginsenosides, gambogic acid and others have demonstrated significant cytotoxicity to various malignant tumors (Cheong, et al., 2020, Kim, et al., 2004, Wang, et al., 2021, Zhang, D., et al., 2020). It was reported that 65% of anticancer drugs currently on the market come from natural products (Newman&Cragg, 2016).

In view of the key roles of UHRF1 in cancer initiation and progression, several natural compounds extracted from the Chinese herbals have been reported to target UHRF1, such as Luteolin (30, 40, 5, 7-tetrahydroxyflavone) (Krifa, et al., 2014), Epigallocatechin-3-gallate (EGCG) (Achour, et al., 2013), Thymoquinone (Alhosin, et al., 2010), Limoniastrum guyonianum aqueous gall extract (Krifa, et al., 2013), red wine polyphenolic extract (RWP) (Sharif, et al., 2010), Bilberry extract (Antho 50) (Alhosin, et al., 2015), Naphthazarin (DHNQ) (Chow, et al., 2018) and Hinokitiol (4-isopropyltropolone) (Seo, et al., 2017).

In this present study, we screened a natural molecule bank for PCa treatment by using network pharmacology together with molecular docking, and Diosgenin (DSG) was identified as a novel UHRF1-targeted specific inhibitor. Furthermore, we explored its involved anticancer mechanism by using the *in vitro* and *in vivo* assays. DSG induced UHRF1 protein degradation, and then reduced the level of genomic DNA methylation, and re-activated the expression of TSGs, thereby resulted in cell cycle arrest and cell senescence. This present study provided a promising strategy to discover new molecule-targeting drug from natural compounds.

2 | MATERIALS AND METHODS

2.1 | Data Mining from the Cancer Genome Atlas (TCGA) Database

mRNA-seq and clinical data of 481 primary prostate adenocarcinoma tissues and 51 non-malignant controls were acquired from the TCGA-PRAD dataset (<https://portal.gdc.cancer.gov/>). After excluding those cases with incomplete data of TNM stage and survival, 397 patients were finally enrolled in this study. After normalizing raw data, we identified the differential expression genes of read counts between the normal controls and PRAD tissues using the edgeR package in R. Adjusted p value < 0.05 and $|\log_2(\text{fold change})| > 1$ were defined as the threshold. UHRF1 expression among different clinicopathological groups was analyzed using Student's t-test. Receiver operating characteristic (ROC) curve was used to judge the diagnostic value of UHRF1 for PRAD, and the area under the curve (AUC) was calculated. Recurrence free survival (RFS) analysis was calculated by GEPIA2 (<http://gepia2.cancer-pku.cn/>) (Tang, et al., 2017).

2.2 | Screening of small molecules

We searched the Traditional Chinese Medicine Systems Pharmacology Database (TCMSP) and Analysis Platform database (<https://old.tcmsp-e.com/tcmsp.php>) for the active ingredients in the most commonly 36 botanicals used for PCa treatment in the clinic (Ru, et al., 2014, wanli&zhong, 2018). We then screened the

target molecules using the following criteria. 1) The molecules exist in four or more botanicals, and 2) the molecules cannot be synthesized by human body. Finally, 75 small molecules were identified by using the online website UPSET (<https://cloud.oebiotech.cn/task/detail/upset/>).

2.3 | Network pharmacology together with molecular docking

The structures of 75 small molecules were obtained from the PubChem database (<https://pubchem.ncbi.nlm.nih.gov/>). The details could be found in the Supplementary Table 1. The protein crystal structures of five domains of UHRF1 were downloaded from the protein database (<http://www.rcsb.org/pdb/home/home.do>) (PDB: 3ASL, PDB: 3FL2, PDB: 6W92, PDB: 2FAZ and PDB: 3BI7). Before molecule docking, the structure of target proteins was pre-processed using AutoTools and PYMOL, including removal of water molecules and ligands, addition of hydrogen, etc. Then, the size of grid matrix for blind docking was adjusted such that the protein molecules had completely been covered. Finally, the candidate ingredients were chosen for molecular docking using Autodock Vina software (Trott&Olson, 2010), and the results were visualized using PYMOL. Based on the lowest binding energy score, results were represented as heatmaps by R package pheatmap.

2.4 | Cells culture and siRNA transfection

LNCaP, C4-2, DU145 and PC3 cells were cultured in RPMI-1640 media (Gibco) supplemented with 10% fetal bovine serum (FBS) and antibiotics (100 U/mL penicillin and 100 mg/mL streptomycin) at 37 °C in a 5% CO₂ humidified atmosphere. siRNA transfection was performed using a Mirus Transfection Kit according to the manufacturer's protocol (Mirus, Madison, WA). The siRNA sequences used for UHRF1 knockdown were (5'-3'): GCGCUGGCUCUCAACUGCU.

2.5 | Antibodies and chemicals

The antibodies and chemicals used in the study include anti-UHRF1 (Proteintech, 21402-1-AP), anti-His (Genscript, A00186), anti-HA (Cell Signal Technology, CST, 3724), anti-5-Methylcytosine (CST, 28692), anti-p21 (CST, 2947), anti-HDAC1 (CST, 34589) and anti-β-actin (Abclonal, AC004). Cycloheximide (CHX) was purchased from CST, MG132 was purchased from Selleck Chemicals (Houston, Texas, USA), L7G and DSG were purchased from MedChemExpress (MCE, Shanghai, China).

2.6 | Cell viability assays

Cells were cultured in 96-well flat-bottomed microtiter plates (5000 cells per well), and treated with DSG for 48 h. CCK8 stock solution was added to each well according to the manufacturer's instructions, and the plate was incubated at 37 °C for 1 h. Cell viability was assessed by measuring the absorbance at 450 nm using a microplate reader (Multiskan-GO, Thermo Fisher Scientific, China).

2.7 | Western blotting and Real-time PCR assay

Cells were washed three times with cold PBS and lysed in RIPA buffer, and then centrifuged for 15 min to collect supernatant. The protein concentration was measured using a BCA assay kit. The protein levels were assessed by western blotting.

The total RNA was extracted from PCa cells, or xenograft tumor tissues following the RNAiso Plus manufacturer's protocol (Takara Bio, Beijing, China). The concentration and quality of RNA samples were determined, and then reverse-transcribed to cDNA. The mRNA levels of genes were measured by real-time PCR system according to the manufacturer's instructions. Primers for RT-PCR were: *UHRF1* : 5'-AGGTGGTCATGCTCAACTACA-3' (forward), 5'-CACGTTGGCGTAGAGTTCCC-3' (reverse). *p16* : 5'-CGGTCGGAGGCCGATCCAG-3' (forward), 5'-GCGCCGTGGAGCAGCAGCAGCT-3' (reverse). *p21* : 5'-ATGGAACCTCGACTTTGTCACC-3' (forward), 5'-AGGCACAAGGGTACAAGACAGT-3' (reverse). *LXN* : 5'-ACAAGCCAGCATGGAGGATA-3' (forward), 5'-TCAGCTGTGCAGTTCACCTT-3' (reverse).

2.8 | *In vivo* ubiquitination assay

Cells were transfected with the indicated plasmids, and treated with DSG for 48 h and followed by the treatment of 50 μ M MG132 for additional 6 h. The cells were lysed in RIPA buffer and boiled at 100 °C for 10 min. The cell lysates were centrifuged at 12,000 g for 15 min. UHRF1 protein was immunoprecipitated with anti-His antibody on a rotator at 4 °C for 12 h, and the immune complexes were incubated with protein A/G-magnetic beads. After being washed three times, the immunocomplex was subjected to SDS-PAGE and the ubiquitination levels were assessed by western blotting.

2.9 | Dot blot analysis

Genomic DNA was extracted using a genomic DNA purification kit according to the manufacturer's protocol (CoWin Biosciences, Beijing, China). The extracted DNA was denatured at 95 °C for 10 min, and then 100 ng DNA was blotted onto nitrocellulose membrane and fixed at 85 °C for 30 min. The cross-linked nylon membrane was incubated in blocking solution (5% BSA) for 1 h at room temperature, and hybridized with anti-5-mC overnight at 4 °C. The membrane was incubated with the secondary antibody at room temperature for 1 h, and detected by chemiluminescent detection reagents. Methylene blue intensity of DNA dots was used to determine the amount of genomic DNA methylation.

2.10 | Cellular senescence assay

Cellular senescence was assessed by Senescence-Associated β -Galactosidase Staining Kit (Beyotime Biotechnology, Beijing, China) according to the manufacturer's instructions. Cells were treated with DSG for 3 days, the cells were washed twice with PBS, fixed at room temperature for 10-15 min, and incubated with fresh β -gal staining solution at 37 °C overnight. The β -gal-positive cells were monitored under a microscope.

2.11 | Cell cycle analysis

Cells were treated with DSG for 72 h, and were fixed in 70% ethanol in PBS at 4 °C for 24 h. The supernatant was discarded after centrifugation at 1,500 rpm for 10 minutes. For cell cycle analysis, cells were re-suspended in 1 mL PBS containing propidium iodide (PI) incubated at room temperature avoiding light for 30 min. Cell cycle distribution was analyzed by flow cytometer (Attune NxT, Thermo Fisher Scientific, China).

2.13 | In vivo animal study

All animal experiments were approved by the Institutional Animal Care and Use Committee (IACUC) at the Institute of Laboratory Animal Science (Number:00287876), Guangdong Pharmaceutical University (Guangzhou, China), and conformed to the relevant regulatory standards. Nude mice (4-5weeks old, male) were kept for one week before the start of the experiment to adopt the conditions. All animals were housed in airconditioned rooms (22 ± 2 °C, 50% humidity and 12 h of dark or light cycles), and had free access to standard drinking water.

The tumor xenografts were induced by subcutaneously inoculating DU145 cells ($5 \times 10^6 \cdot 100^{-1}$ μ L) into the left flank region of mice. Mice were randomly divided into 3 groups; a control group, a low-dose group (DSG 40 mg/kg), and a high-dose group (DSG 80 mg/kg). The control group was gavaged with 0.5% CMC-Na. Tumor size was measured with calipers every three days. and the tumor volumes were calculated according to the following formula: $V = (\text{max diameter}) \times (\text{min diameter})^2 \cdot 2^{-1}$. The tumor xenografts were isolated at the endpoint of experiment, and the tumors were then photographed and weighed. The liver and kidney tissues were fixed in 10% buffered formalin and embedded in paraffin for H&E staining.

2.13 | Statistical analysis

All statistical analyses were performed using GraphPad Prism8 (v8.0.2). The results are expressed as means \pm standard deviation. The significance of differences among groups was assessed using one-way analysis of variance with post hoc Bonferroni test. Paired data were analyzed using the paired-samples t test. * $p < 0.05$, ** $p < 0.01$, *** $p < 0.001$, and**** $p < 0.0001$ denoted statistical significance. The Kaplan-Meier provides a method for estimating the survival curves, and the log-rank test provides a statistical comparison of two groups.

3 | RESULTS

3.1 | Aberrant overexpression of UHRF1 in PCa tissues and promoted PCa progression

To assess whether UHRF1 is associated with PCa progression, we compared their expression levels in tumoral and normal tissues using TCGA database. The UHRF1 mRNA level was dramatically up-regulated in PCa tissues (n=481) compared with normal tissues (n = 51) ($P < 0.0001$) (Fig. 1a), and the mRNA level of UHRF1 was positively correlated with the TNM stages of PCa (Fig.1b). More importantly, Knockdown of UHRF1 in PCa cells with siRNAs reduced the number of cells clonogenicity, suggesting that UHRF1 plays an important role in tumor growth and progression (Fig.1c). We further analyzed the correlation of UHRF1 mRNA level with the morbidity of PCa patients, and the diagnostic value of UHRF1 upregulation for PCa was confirmed by ROC curves (AUC= 0.747, $P < 0.0001$) (Fig. 1d). Finally, we analyzed the correlation between UHRF1 mRNA levels and PCa patient recurrence-free survival (RFS), the results showed that the mRNA level of UHRF1 was negatively correlated with RFS (Fig.1e). All these results confirmed the oncogene role of UHRF1, which contributes to the tumorigenesis and progression of PCa.

3.2 | A small molecule compound targeting UHRF1 protein was identified using molecule docking approach.

UHRF1 has become a potential drug target for PCa, which inspired us to search for small molecule inhibitors targeting UHRF1 protein. From the most commonly used 36 traditional Chinese medicines for the treatment of PCa in China (wanli&hong, 2018), we screened 75 small molecule compounds using TCMSP database, and then performed molecular docking with the five crystal structure domains of UHRF1 that were obtained from the PDB database. The heatmap shows the binding energy of the docking of 75 small molecules on 5 domains of UHRF1 by using autodock vina. After performing the hierarchical clustering analysis using the pheatmap R package (Fig. 2a). Among them, DSG and Luteolin 7-glucoside (L7G) have the best comprehensive scores. L7G is a flavonoid compound (Fig. 2b), DSG is a steroidal saponin (Fig. 2c). To clarify how small molecule compounds L7G and DSG interact with UHRF1 protein, we re-analyzed the molecular docking results, and predicted the most binding possibility of small molecules with protein domains. The results demonstrate that L7G binds the UBL domain of UHRF1 (Fig. 2d-f), while DSG binds the TTD domain of UHRF1 (Fig. 2e-g). We focused on L7G and DSG for further studies in the subsequent experiments.

3.3 | DSG induced UHRF1 protein degradation, but did not reduce mRNA levels

To investigate the effects of L7G and DSG on UHRF1 protein, we treated PC3 cells with different concentrations of DSG or L7G for 48 hours, and assessed the protein and mRNA levels of UHRF1. As shown in Fig. 3a and Fig. 3b, L7G simultaneously reduced the levels of protein and mRNA of UHRF1, while DSG only reduced the protein of UHRF1, did not reduce the mRNA level. Consistently, DSG dramatically induced UHRF1 protein degradation, but did not change mRNA levels in C4-2 and DU145 (Fig. 3c-d). We speculated that DSG might directly bind to UHRF1 protein through TTD domain, and induced protein degradation of UHRF1. The results indicated that DSG reduced UHRF1 expression through a post-translational mechanism. Additionally, DSG greatly elevated the protein level of p21, a typical downstream molecule of UHRF1, but had no impact on the protein level of HDAC1. Since HDAC1 inhibitors have been reported to elevate p21 level (Lagger, et al., 2002), we speculate that DSG specifically reduced UHRF1 expression in PCa cells.

3.4 | DSG induced UHRF1 protein degradation through the ubiquitin-proteasome system pathway

Next, we investigated the impact of DSG on UHRF1 protein stability by testing the half-time of UHRF1 protein. The protein synthesis was inhibited by cycloheximide (CHX), and then UHRF1 protein was assessed at continuous time points. DSG reduced the half-life of UHRF1 protein in C4-2 and DU145 cells (Fig. 4a-b). suggesting that DSG promoted the protein degradation of UHRF1. It is reported that the ubiquitin-proteasome pathway is the major reason of UHRF1 protein degradation (Ma, et al., 2012). We treated PCa cells with DSG for 40h, and then followed by the treatment of a ubiquitination-proteasome pathway inhibitor MG132 for additional 8h. The data showed that DSG induced the protein degradation of UHRF1, while the

protein degradation was reversed by MG132 (Fig. 4c-d). The results were further validated by the *in vivo* ubiquitination assay. The plasmids of HA-ubiquitin and UHRF1-His were co-transfected into C4-2 or PC3 cells, and then treated with different doses of DSG. UHRF1 protein was immunoprecipitated with anti-His antibody, and poly-ubiquitinated UHRF1 was assessed with anti-HA antibody. The results showed that the ubiquitination level of UHRF1 protein increased with DSG concentrations (Fig. 4e-f). Taken together, these results validated that DSG promoted the protein degradation of UHRF1 through the ubiquitin-proteasome system.

3.5 | DSG inhibited cell survival by inducing UHRF1 protein degradation.

It was reported that UHRF1 depletion remarkably decreased cancer cell proliferation and viability (Liu, et al., 2020). Since DSG induced UHRF1 protein degradation, we tested the impacts of DSG on PCa cell proliferation and viability using CCK-8 assays, and calculated the 50% inhibitory concentrations. DSG inhibited cell proliferation and viability of PCa cell lines in a dose-dependent manner. More importantly, the inhibitory effect of DSG on PCa cells is highly and positively correlated with the expression levels of UHRF1 (Fig. 5a-b). In the effort to validate whether the inhibitory effect of DSG is attributed to UHRF1 inhibition, we re-examined the inhibitory effect of DSG on cell viability of DU145 and PC3 cells when UHRF1 was silenced with siRNAs. The results showed that UHRF1 knockdown attenuated the inhibitory effect of DSG (Fig. 5c-e), suggesting that DSG inhibited cell proliferation and viability of PCa cells by specifically targeting UHRF1 protein.

3.6 | DSG reduced the genomic DNA methylation levels, and re-activated the expression of TSGs, resulting in cell cycle arrest and cellular senescence of PCa cells.

It has been reported that UHRF1 depletion reduced the genomic DNA methylation levels, and re-activated the expression of TSGs, resulting in cell cycle arrest and cellular senescence (Yang, et al., 2017, Kong, et al., 2019a). We validated whether DSG made the same effect on PCa cells. We treated cells with DSG for 5 days, and assessed the genomic DNA methylation levels using DNA dot blotting. As expected, DSG decreased the genomic DNA methylation levels (Fig. 6a). Recent emerging evidences have suggested that DNA hypomethylation might re-activate the expression of TSGs (Zhang&Xu, 2017). We next examined the impact of DSG on the expression levels of TSGs. The data showed that DSG increased the mRNA levels of such TSGs as *p16*, *p21* and *LXN* (Fig. 6b). As we knew that p16 and p21 were important cell cycle inhibitor and biomarkers of cellular senescence (Scott, et al., 2017, Chen, et al., 2014, Sharma, et al., 2020). We further examined the influences of DSG on cell cycle and cell senescence. As expected, DSG induced cell cycle arrest in S phase, and induced cell senescence (Fig. 6c-d). These results indicated that DSG, by inducing the protein degradation of UHRF1, reduced the genomic DNA methylation levels and re-activated the expression of TSGs, resulting in cell cycle arrest, and inducing cellular senescence of PCa cells.

3.7 | DSG inhibited the growth of PCa xenografts.

Epigenetic suppression of TSGs and escape of cellular senescence are two critical hallmarks of tumor progression (Hanahan&Weinberg, 2011). Therefore, development of new therapeutics by targeting these two hallmarks is therefore ideal avenue. Based on the *in vitro* findings that DSG is effective in reactivating TSGs expression and triggering cell senescence, we then examined the therapeutic efficacy of DSG on the pre-existing *in vivo* tumor xenografts. As expected, DSG inhibited the growth of DU145 tumor xenografts in a dose-dependent manner (Fig. 7a-b-c-d). Consistent with the *in vitro* data, DSG increased the expression of such typical TSGs as *p16*, *LXN* and *p21* inside the tumor nodes (Fig. 7e). Compared to the control mice, we found no statistically significant change in the body weight of DSG-treated mice (Fig. 6f). Meanwhile, Histopathological examination showed DSG treatment did not induce obvious liver and kidney toxicity (Fig. 6g). DSG demonstrated strong anti-PCa efficacy in both *in vitro* cell lines and *in vivo* tumor xenografts, and the inhibitory effect is closely correlated with the protein levels of UHRF1, suggesting a high tumor specificity.

4 | DISCUSSION

Under normal physiological conditions, UHRF1 is highly expressed only in actively proliferating cells and tissues, and its level is modified with cell cycle progression (Yamashita, et al., 2018, Mancini, et al., 2021). UHRF1 protein steadily elevates in G1/S phase, and reaches the peak at mid S-phase, when heterochromatic regions are replicated, and it is down-regulated at the end of M phase (Mancini, et al., 2021). However, in tumor cells, aberrant overexpression of UHRF1 results in the dysregulation of cell cycle. UHRF1 has been regarded as a typical oncogene, and significantly promotes tumorigenesis and cancer progress (Ashraf, et al., 2017). In this present study, we found that UHRF1 was highly expressed in PCa tissues, and the level increased with the elevation of PCa grades, and was negatively correlated with the survival of PCa patients (Fig 1a-b, and e), suggesting that UHRF1 as an oncogene promotes the initiation and progress of PCa.

UHRF1 facilitates the establishment and maintenance of DNA methylation patterns in mammalian cells, and induces the silencing of TSGs expression in tumors (Kong, et al., 2019b). In the present manuscript, knockdown of UHRF1 in PCa cells inhibited cell clonogenicity (Fig 1c). The results indicated that UHRF1 is a potential therapeutic target for PCa, but no specific inhibitor of UHRF1 has been registered in clinical trials. It has been reported that currently 65% of anticancer drugs on the market derived from the monomer structures of natural products (Newman&Cragg, 2016). According to the Compendium of Materia Medica, the proportion of botanical medicinal materials in TCM is approximately 70%. Since UHRF1 plays a critical role in the development and progression of PCa, and TCM has a long history and rich experience in the treatment of PCa, we speculate that some monomer components from botanical medicinal materials in TCM probably make anti-PCa effect by inhibiting UHRF1-mediated pathway. Therefore, we for the first time screened a natural molecule bank for PCa treatment by using network pharmacology together with molecular docking. Diosgenin (DSG) was identified as a novel UHRF1 specific inhibitor from 36 traditional Chinese medicines (Fig 2). DSG demonstrated significant anti-cancer therapeutic efficacy in the *In vitro* cell lines and *in vivo* tumor xenograft models (Fig 5 and Fig 7).

Further mechanism investigations clarified that DSG induced the protein degradation of UHRF1 through the ubiquitination-proteasome pathway (Fig 4). DSG reduced genomic DNA methylation and reactivated the expression of TSGs, resulting in cell cycle arrest and inducing cell senescence (Fig 6). It has been reported that USP7 is a deubiquitinase removing ubiquitin a 76 amino acid protein that is added onto lysines in UHRF1 protein, and sustaining its stability (Felle, et al., 2011, Turnbull, et al., 2017). We investigated the molecular mechanism by which DSG induced UHRF1 protein degradation. Beyond our expectations, compared to the working doses of DSG for cytotoxicity, an extremely high concentration (60uM) was required to destroy the protein interaction of UHRF1 and USP7 (Supplementary Fig 1). Therefore, the molecular mechanism by which DSG induce UHRF1 protein degradation needs further exploration in our future studies.

Altogether, we for the first time identified DSG as a novel UHRF1 specific inhibitor for PCa treatment after screening a natural molecule bank by using network pharmacology together with molecular docking. We then found that DSG induced UHRF1 protein degradation through the ubiquitin-proteasome pathway. UHRF1 protein degradation reactivated the expression of TSGs, resulting in cell cycle arrest and inducing cell senescence. By using network pharmacology together with molecular docking in this study, we will identify more specific small molecule inhibitors targeting specific oncoproteins from natural products in TCM. These molecule-targeted inhibitors have great potentials for new drug development after structural modifications, and being tested the therapeutic efficacy, safety and pharmaceutical characters.

ACKNOWLEDGMENTS

This work was supported by grants from the National Natural Science Foundation of China (NSFC, 81572542 and NSFC, 81874096), and Research Project of Key Discipline of Guangdong Province (2019GDXXK0010), Science and Technology Program of Guangzhou City (The roles of AR mitochondrial translocation in the development of anti-androgen drug resistance in prostate cancer), National Key Specialty Construction Project of Clinical Pharmacy, High Level Clinical Key Specialty of Clinical Pharmacy in Guangdong Province.

ACKNOWLEDGEMENTS

AUTHOR CONTRIBUTIONS

RT designed and performed the experiments, collected experimental data and wrote the paper draft; YCP helped designed the study, performed experiments and the paper writing; LYD assisted Dot blot assay and animal experiments; YHL, LLY took part and assisted in some experiments; YMF, TGD made constructive suggestions on the experimental design and data analysis; XL provided the laboratory where experiments being conducted, financial supports, designed the study, and finished final writing of the paper.

DECLARATION OF TRANSPARENCY AND SCIENTIFIC RIGOUR

This Declaration acknowledges that this paper adheres to the principles for transparent reporting and scientific rigour of preclinical research as stated in the BJP guidelines for Design Animal Experimentation and as recommended by funding agencies, publishers and other organizations engaged with supporting research

COMPETING INTEREST

The authors declare that there are no conflicts of interest.

DATA AVAILABILITY STATEMENT

The data that support the findings of this study are available from the corresponding author upon reasonable request.

ORCID

Xiong Li: <https://orcid.org/0000-0001-6147-1090>

REFERENCES

- R. L. Siegel, K. D. Miller, H. E. Fuchs, A. Jemal, Cancer Statistics, 2021. (2021). *CA Cancer J Clin*, 1, 7-33. <http://dx.doi.org/10.3322/caac.21654>
- M. S. Litwin, H. J. Tan, The Diagnosis and Treatment of Prostate Cancer: A Review. (2017). *Jama*, 24, 2532-2542. <http://dx.doi.org/10.1001/jama.2017.7248>
- P. A. Watson, V. K. Arora, C. L. Sawyers, Emerging mechanisms of resistance to androgen receptor inhibitors in prostate cancer. (2015). *Nat Rev Cancer*, 12, 701-11. <http://dx.doi.org/10.1038/nrc4016>
- R. Gao, D. K. Price, W. L. Dahut, E. Reed, W. D. Figg, Genetic polymorphisms in XRCC1 associated with radiation therapy in prostate cancer. (2010). *Cancer Biol Ther*, 1, 13-8. <http://dx.doi.org/10.4161/cbt.10.1.12172>
- K. Ruggero, S. Farran-Matas, A. Martinez-Tebar, A. Aytes, Epigenetic Regulation in Prostate Cancer Progression. (2018). *Curr Mol Biol Rep*, 2, 101-115. <http://dx.doi.org/10.1007/s40610-018-0095-9>
- K. Arita, S. Isogai, T. Oda, M. Unoki, K. Sugita, N. Sekiyama, K. Kuwata, R. Hamamoto, H. Tochio, M. Sato, M. Ariyoshi, M. Shirakawa, Recognition of modification status on a histone H3 tail by linked histone reader modules of the epigenetic regulator UHRF1. (2012). *Proc Natl Acad Sci U S A*, 32, 12950-5. <http://dx.doi.org/10.1073/pnas.1203701109>
- S. A. Bert, M. D. Robinson, D. Strbenac, A. L. Statham, J. Z. Song, T. Hulf, R. L. Sutherland, M. W. Coolen, C. Stirzaker, S. J. Clark, Regional activation of the cancer genome by long-range epigenetic remodeling. (2013). *Cancer Cell*, 1, 9-22. <http://dx.doi.org/10.1016/j.ccr.2012.11.006>
- D. Patnaik, P. O. Esteve, S. Pradhan, Targeting the SET and RING-associated (SRA) domain of ubiquitin-like, PHD and ring finger-containing 1 (UHRF1) for anti-cancer drug development. (2018). *Oncotarget*, 40, 26243-26258. <http://dx.doi.org/10.18632/oncotarget.25425>
- J. Yang, K. Liu, J. Yang, B. Jin, H. Chen, X. Zhan, Z. Li, L. Wang, X. Shen, M. Li, W. Yu, Z. Mao, PIM1 induces cellular senescence through phosphorylation of UHRF1 at Ser311. (2017). *Oncogene*, 34, 4828-4842. <http://dx.doi.org/10.1038/onc.2017.96>

- H. Chen, H. Ma, H. Inuzuka, J. Diao, F. Lan, Y. G. Shi, W. Wei, Y. Shi, DNA damage regulates UHRF1 stability via the SCF(β -TrCP) E3 ligase. (2013). *Mol Cell Biol*, 6, 1139-48. <http://dx.doi.org/10.1128/mcb.01191-12>
- A. Beck, F. Trippel, A. Wagner, S. Joppien, M. Felle, C. Vokuhl, T. Schwarzmayr, T. M. Strom, D. von Schweinitz, G. Langst, R. Kappler, Overexpression of UHRF1 promotes silencing of tumor suppressor genes and predicts outcome in hepatoblastoma. (2018). *Clin Epigenetics*, 27. <http://dx.doi.org/10.1186/s13148-018-0462-7>
- H. J. Jung, H. O. Byun, B. A. Jee, S. Min, U. W. Jeoun, Y. K. Lee, Y. Seo, H. G. Woo, G. Yoon, The Ubiquitin-like with PHD and Ring Finger Domains 1 (UHRF1)/DNA Methyltransferase 1 (DNMT1) Axis Is a Primary Regulator of Cell Senescence. (2017). *J Biol Chem*, 9, 3729-3739. <http://dx.doi.org/10.1074/jbc.M116.750539>
- P. A. Pérez-Mancera, A. R. Young, M. Narita, Inside and out: the activities of senescence in cancer. (2014). *Nat Rev Cancer*, 8, 547-58. <http://dx.doi.org/10.1038/nrc3773>
- X. L. Su, J. W. Wang, H. Che, C. F. Wang, H. Jiang, X. Lei, W. Zhao, H. X. Kuang, Q. H. Wang, Clinical application and mechanism of traditional Chinese medicine in treatment of lung cancer. (2020). *Chin Med J (Engl)*, 24, 2987-2997. <http://dx.doi.org/10.1097/CM9.0000000000001141>
- M. J. Hsieh, M. K. Chen, Y. Y. Yu, G. T. Sheu, H. L. Chiou, Psoralen reverses docetaxel-induced multidrug resistance in A549/D16 human lung cancer cells lines. (2014). *Phytomedicine*, 7, 970-7. <http://dx.doi.org/10.1016/j.phymed.2014.03.008>
- L. Zhang, B. Yan, S. Meng, L. Zhou, Y. Xu, W. Du, L. Shan, Theaflavin Induces Apoptosis of A375 Human Melanoma Cells and Inhibits Tumor Growth in Xenograft Zebrafishes Through P53- and JNK-Related Mechanism. (2020). *Front Pharmacol*, 1317. <http://dx.doi.org/10.3389/fphar.2020.01317>
- P. Duan, Z. M. Wang, [Clinical study on effect of Astragalus in efficacy enhancing and toxicity reducing of chemotherapy in patients of malignant tumor]. (2002). *Zhongguo Zhong Xi Yi Jie He Za Zhi*, 7, 515-7. <http://dx.doi.org/>
- Y. Zhang, Z. Wu, H. Yu, H. Wang, G. Liu, S. Wang, X. Ji, Chinese Herbal Medicine Wenxia Changfu Formula Reverses Cell Adhesion-Mediated Drug Resistance via the Integrin β 1-PI3K-AKT Pathway in Lung Cancer. (2019). *J Cancer*, 2, 293-304. <http://dx.doi.org/10.7150/jca.25163>
- D. H. J. Cheong, D. W. S. Tan, F. W. S. Wong, T. Tran, Anti-malarial drug, artemisinin and its derivatives for the treatment of respiratory diseases. (2020). *Pharmacol Res*, 104901. <http://dx.doi.org/10.1016/j.phrs.2020.104901>
- H. S. Kim, E. H. Lee, S. R. Ko, K. J. Choi, J. H. Park, D. S. Im, Effects of ginsenosides Rg3 and Rh2 on the proliferation of prostate cancer cells. (2004). *Arch Pharm Res*, 4, 429-35. <http://dx.doi.org/10.1007/bf02980085>
- H. Wang, Y. Zheng, Q. Sun, Z. Zhang, M. Zhao, C. Peng, S. Shi, Ginsenosides emerging as both bifunctional drugs and nanocarriers for enhanced antitumor therapies. (2021). *J Nanobiotechnology*, 1, 322. <http://dx.doi.org/10.1186/s12951-021-01062-5>
- D. Zhang, Y. Chu, H. Qian, L. Qian, J. Shao, Q. Xu, L. Yu, R. Li, Q. Zhang, F. Wu, B. Liu, Q. Liu, Antitumor Activity of Thermosensitive Hydrogels Packaging Gambogic Acid Nanoparticles and Tumor-Penetrating Peptide iRGD Against Gastric Cancer. (2020). *Int J Nanomedicine*, 735-747. <http://dx.doi.org/10.2147/IJN.S231448>
- D. J. Newman, G. M. Cragg, Natural Products as Sources of New Drugs from 1981 to 2014. (2016). *J Nat Prod*, 3, 629-61. <http://dx.doi.org/10.1021/acs.jnatprod.5b01055>
- M. Krifa, L. Leloup, K. Ghedira, M. Mousli, L. Chekir-Ghedira, Luteolin induces apoptosis in BE colorectal cancer cells by downregulating calpain, UHRF1, and DNMT1 expressions. (2014). *Nutr Cancer*, 7, 1220-7. <http://dx.doi.org/10.1080/01635581.2014.951729>

- M. Achour, M. Mousli, M. Alhosin, A. Ibrahim, J. Peluso, C. D. Muller, V. B. Schini-Kerth, A. Hamiche, S. Dhe-Paganon, C. Bronner, Epigallocatechin-3-gallate up-regulates tumor suppressor gene expression via a reactive oxygen species-dependent down-regulation of UHRF1. (2013). *Biochem Biophys Res Commun*, 1, 208-12. <http://dx.doi.org/10.1016/j.bbrc.2012.11.087>
- M. Alhosin, A. Abusnina, M. Achour, T. Sharif, C. Muller, J. Peluso, T. Chataigneau, C. Lugnier, V. B. Schini-Kerth, C. Bronner, G. Fuhrmann, Induction of apoptosis by thymoquinone in lymphoblastic leukemia Jurkat cells is mediated by a p73-dependent pathway which targets the epigenetic integrator UHRF1. (2010). *Biochem Pharmacol*, 9, 1251-60. <http://dx.doi.org/10.1016/j.bcp.2009.12.015>
- M. Krifa, M. Alhosin, C. D. Muller, J. P. Gies, L. Chekir-Ghedira, K. Ghedira, Y. Mély, C. Bronner, M. Mousli, *Limoniastrum guyonianum* aqueous gall extract induces apoptosis in human cervical cancer cells involving p16 INK4A re-expression related to UHRF1 and DNMT1 down-regulation. (2013). *J Exp Clin Cancer Res*, 1, 30. <http://dx.doi.org/10.1186/1756-9966-32-30>
- T. Sharif, C. Auger, M. Alhosin, C. Ebel, M. Achour, N. Etienne-Selloum, G. Fuhrmann, C. Bronner, V. B. Schini-Kerth, Red wine polyphenols cause growth inhibition and apoptosis in acute lymphoblastic leukemia cells by inducing a redox-sensitive up-regulation of p73 and down-regulation of UHRF1. (2010). *Eur J Cancer*, 5, 983-94. <http://dx.doi.org/10.1016/j.ejca.2009.12.029>
- M. Alhosin, A. J. León-González, I. Dandache, A. Lelay, S. K. Rashid, C. Kevers, J. Pincemail, L. M. Fornecker, L. Mauvieux, R. Herbrecht, V. B. Schini-Kerth, Bilberry extract (Antho 50) selectively induces redox-sensitive caspase 3-related apoptosis in chronic lymphocytic leukemia cells by targeting the Bcl-2/Bad pathway. (2015). *Sci Rep*, 8996. <http://dx.doi.org/10.1038/srep08996>
- M. Chow, L. Gao, J. D. MacManiman, V. T. Bicozza, B. H. Chang, J. J. Alumkal, J. W. Tyner, Maintenance and pharmacologic targeting of ROR1 protein levels via UHRF1 in t(1;19) pre-B-ALL. (2018). *Oncogene*, 38, 5221-5232. <http://dx.doi.org/10.1038/s41388-018-0299-8>
- J. S. Seo, Y. H. Choi, J. W. Moon, H. S. Kim, S. H. Park, Hinokitiol induces DNA demethylation via DNMT1 and UHRF1 inhibition in colon cancer cells. (2017). *BMC Cell Biol*, 14. <http://dx.doi.org/10.1186/s12860-017-0130-3>
- Z. Tang, C. Li, B. Kang, G. Gao, C. Li, Z. Zhang, GEPIA: a web server for cancer and normal gene expression profiling and interactive analyses. (2017). *Nucleic Acids Res*, W1, W98-W102. <http://dx.doi.org/10.1093/nar/gkx247>
- J. Ru, P. Li, J. Wang, W. Zhou, B. Li, C. Huang, P. Li, Z. Guo, W. Tao, Y. Yang, X. Xu, Y. Li, Y. Wang, L. Yang, TCMSP: a database of systems pharmacology for drug discovery from herbal medicines. (2014). *J Cheminform*, 13. <http://dx.doi.org/10.1186/1758-2946-6-13>
- A. wanli, Y. hong, Analysis on the regularity of prescription of traditional Chinese medicine for the treatment of prostate cancer. (2018). *Pharmacovigilance in China*, 03, 158-162. <http://dx.doi.org/>
- O. Trott, A. J. Olson, AutoDock Vina: improving the speed and accuracy of docking with a new scoring function, efficient optimization, and multithreading. (2010). *J Comput Chem*, 2, 455-61. <http://dx.doi.org/10.1002/jcc.21334>
- G. Lagger, D. O'Carroll, M. Rembold, H. Khier, J. Tischler, G. Weitzer, B. Schuettengruber, C. Hauser, R. Brunmeir, T. Jenuwein, C. Seiser, Essential function of histone deacetylase 1 in proliferation control and CDK inhibitor repression. (2002). *Embo j*, 11, 2672-81. <http://dx.doi.org/10.1093/emboj/21.11.2672>
- H. Ma, H. Chen, X. Guo, Z. Wang, M. E. Sowa, L. Zheng, S. Hu, P. Zeng, R. Guo, J. Diao, F. Lan, J. W. Harper, Y. G. Shi, Y. Xu, Y. Shi, M phase phosphorylation of the epigenetic regulator UHRF1 regulates its physical association with the deubiquitylase USP7 and stability. (2012). *Proc Natl Acad Sci U S A*, 13, 4828-33. <http://dx.doi.org/10.1073/pnas.1116349109>

- Y. Liu, G. Liang, T. Zhou, Z. Liu, Silencing UHRF1 Inhibits Cell Proliferation and Promotes Cell Apoptosis in Retinoblastoma Via the PI3K/Akt Signalling Pathway. (2020). *Pathol Oncol Res*, 2, 1079-1088. <http://dx.doi.org/10.1007/s12253-019-00656-7>
- X. Kong, J. Chen, W. Xie, S. M. Brown, Y. Cai, K. Wu, D. Fan, Y. Nie, S. Yegnasubramanian, R. L. Tiedemann, Y. Tao, R. W. Chiu Yen, M. J. Topper, C. A. Zahnow, H. Easwaran, S. B. Rothbart, L. Xia, S. B. Baylin, Defining UHRF1 Domains that Support Maintenance of Human Colon Cancer DNA Methylation and Oncogenic Properties. (2019a). *Cancer Cell*, 4, 633-648 e7. <http://dx.doi.org/10.1016/j.ccell.2019.03.003>
- W. Zhang, J. Xu, DNA methyltransferases and their roles in tumorigenesis. (2017). *Biomark Res*, 1. <http://dx.doi.org/10.1186/s40364-017-0081-z>
- A. Scott, F. Bai, H. L. Chan, S. Liu, J. M. Slingerland, D. J. Robbins, A. J. Capobianco, X. H. Pei, p16 loss rescues functional decline of Brca1-deficient mammary stem cells. (2017). *Cell Cycle*, 8, 759-764. <http://dx.doi.org/10.1080/15384101.2017.1295185>
- H. Chen, X. Liu, W. Zhu, H. Chen, X. Hu, Z. Jiang, Y. Xu, L. Wang, Y. Zhou, P. Chen, N. Zhang, D. Hu, L. Zhang, Y. Wang, Q. Xu, R. Wu, H. Yu, J. Wang, SIRT1 ameliorates age-related senescence of mesenchymal stem cells via modulating telomere shelterin. (2014). *Front Aging Neurosci*, 103. <http://dx.doi.org/10.3389/fnagi.2014.00103>
- A. Sharma, A. K. Verma, M. Kofron, R. Kudira, A. Miethke, T. Wu, J. Wang, C. R. Gandhi, Lipopolysaccharide Reverses Hepatic Stellate Cell Activation Through Modulation of cMyb, Small Mothers Against Decapentaplegic, and CCAAT/Enhancer-Binding Protein C/EBP Transcription Factors. (2020). *Hepatology*, 5, 1800-1818. <http://dx.doi.org/10.1002/hep.31188>
- D. Hanahan, R. A. Weinberg, Hallmarks of cancer: the next generation. (2011). *Cell*, 5, 646-74. <http://dx.doi.org/10.1016/j.cell.2011.02.013>
- M. Yamashita, K. Inoue, N. Saeki, M. Ideta-Otsuka, Y. Yanagihara, Y. Sawada, I. Sakakibara, J. Lee, K. Ichikawa, Y. Kamei, T. Iimura, K. Igarashi, Y. Takada, Y. Imai, Uhrf1 is indispensable for normal limb growth by regulating chondrocyte differentiation through specific gene expression. (2018). *Development*, 1, 10.1242/dev.157412
- M. Mancini, E. Magnani, F. Macchi, I. M. Bonapace, The multi-functionality of UHRF1: epigenome maintenance and preservation of genome integrity. (2021). *Nucleic Acids Res*, 11, 6053-6068. <http://dx.doi.org/10.1093/nar/gkab293>
- W. Ashraf, A. Ibrahim, M. Alhosin, L. Zaayter, K. Ouararhni, C. Papin, T. Ahmad, A. Hamiche, Y. Mély, C. Bronner, M. Mousli, The epigenetic integrator UHRF1: on the road to become a universal biomarker for cancer. (2017). *Oncotarget*, 31, 51946-51962. <http://dx.doi.org/10.18632/oncotarget.17393>
- X. Kong, J. Chen, W. Xie, S. M. Brown, Y. Cai, K. Wu, D. Fan, Y. Nie, S. Yegnasubramanian, R. L. Tiedemann, Y. Tao, R. W. Chiu Yen, M. J. Topper, C. A. Zahnow, H. Easwaran, S. B. Rothbart, L. Xia, S. B. Baylin, Defining UHRF1 Domains that Support Maintenance of Human Colon Cancer DNA Methylation and Oncogenic Properties. (2019b). *Cancer Cell*, 4, 633-648.e7. <http://dx.doi.org/10.1016/j.ccell.2019.03.003>
- M. Felle, S. Joppien, A. Nemeth, S. Diermeier, V. Thalhammer, T. Dobner, E. Kremmer, R. Kappler, G. Langst, The USP7/Dnmt1 complex stimulates the DNA methylation activity of Dnmt1 and regulates the stability of UHRF1. (2011). *Nucleic Acids Res*, 19, 8355-65. <http://dx.doi.org/10.1093/nar/gkr528>
- A. P. Turnbull, S. Ioannidis, W. W. Krajewski, A. Pinto-Fernandez, C. Heride, A. C. L. Martin, L. M. Tonkin, E. C. Townsend, S. M. Buker, D. R. Lancia, J. A. Caravella, A. V. Toms, T. M. Charlton, J. Lahdenranta, E. Wilker, B. C. Follows, N. J. Evans, L. Stead, C. Alli, V. V. Zarayskiy, A. C. Talbot, A. J. Buckmelter, M. Wang, C. L. McKinnon, F. Saab, J. F. McGouran, H. Century, M. Gersch, M. S. Pittman, C. G. Marshall, T. M. Raynham, M. Simcox, L. M. D. Stewart, S. B. McLoughlin, J. A. Escobedo, K. W. Bair, C. J. Dinsmore, T.

R. Hammonds, S. Kim, S. Urbe, M. J. Clague, B. M. Kessler, D. Komander, Molecular basis of USP7 inhibition by selective small-molecule inhibitors. (2017). *Nature*, 7677, 481-486. <http://dx.doi.org/10.1038/nature24451>

FIGURE LEGENDS

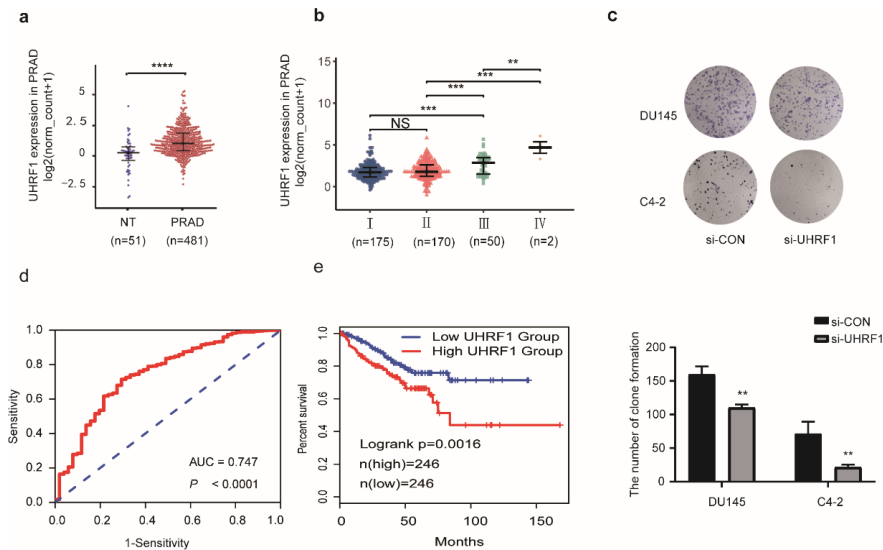


FIGURE 1. Aberrant overexpression of UHRF1 in PCa tissues and promoted PCa progression. **a** Comparison of UHRF1 mRNA levels in PCa (n=481) and normal tissues (n=51). **b** Comparison of UHRF1 mRNA levels in different TNM stage groups of PCa. **c** Colony-formation assays, histogram and statistics indicated the number of colonies per 500 plated cells. Data are representative of three independent experiments and values are expressed in mean ± SD. Significance was determined by Student’s t-test, **p* < 0.01. **d** ROC curve was used to verify the diagnostic value of UHRF1 overexpression for PCa. **e** Recurrence free survival analysis for high (red) and low (blue) expression of UHRF1 in PCa samples from TCGA.

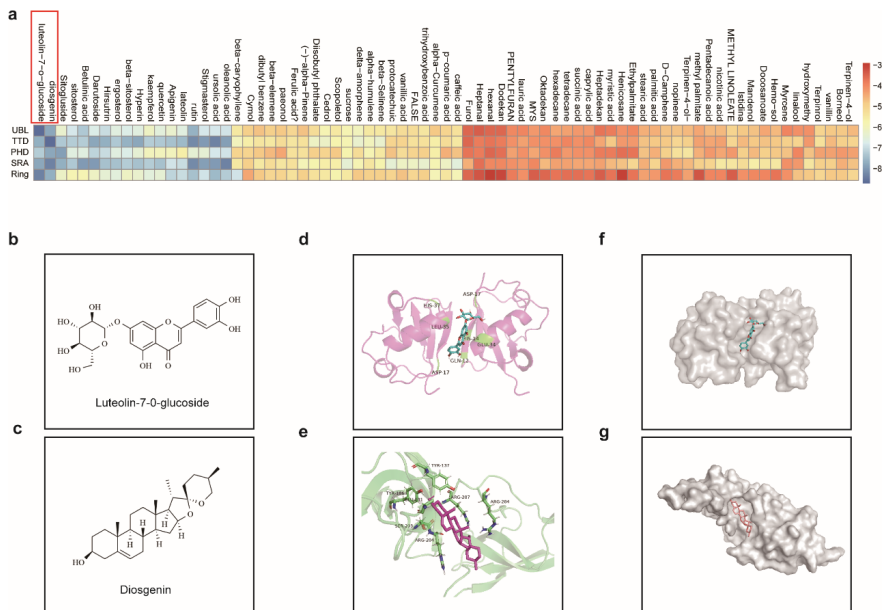


FIGURE 2. A small molecular compound targeting UHRF1 protein was identified using network pharmacology together with molecule docking. **a** Heatmap shows the binding energy of the docking of 75 small molecules on 5 domains of UHRF1 using autodock vina. After performing the hierarchical clustering analysis using the pheatmap R package, 2 small molecules were identified to bind UHRF1 protein based on the lowest comprehensive *in vivo* binding energy. **b-c** Chemical structure of L7G or DSG. **d-e** The structural complex of UHRF1 domain with small molecule based on the minimum binding energy using molecular docking. The UBL domain with L7G (**d**) and the TTD domain with DSG (**e**). **f-g** The potential binding pocket at the interface of the UHRF1(UBL)-L7G complex (**f**) and the UHRF1(TTD)-DSG complex (**g**) was predicted.

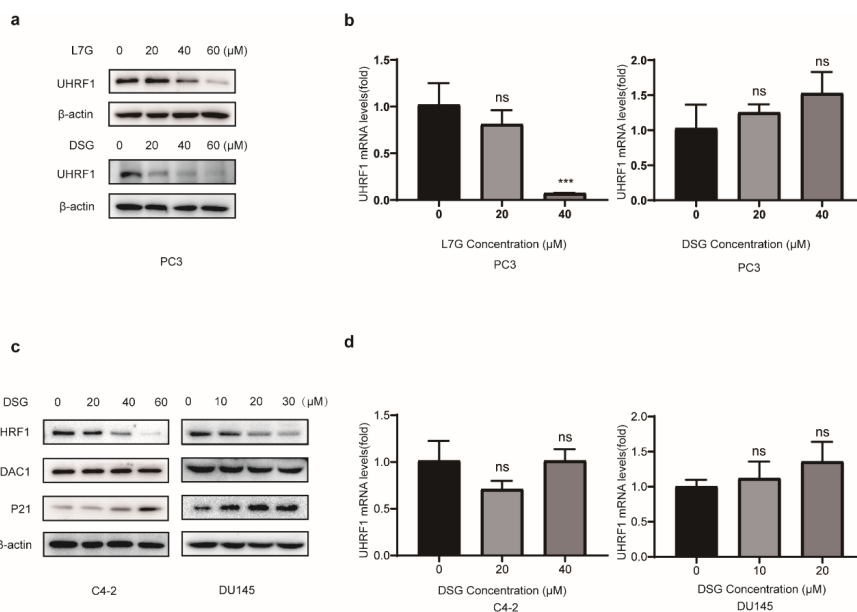


FIGURE 3. DSG induced UHRF1 protein degradation, but did not change mRNA levels. **a** PC3 cells were treated with DSG or L7G at the indicated doses for 48 h, and the proteins were harvested for immunoblotting. **b** PC3 cells were treated with different doses of DSG or L7G for 48 h. The mRNA levels of UHRF1 were analyzed by RT-PCR. β-actin was used as an internal control. **c** C4-2 or DU145 cells were treated with different doses of DSG for 48 h. Cell lysates were harvested and the protein levels were assessed by immunoblotting. **d** C4-2 or DU145 cells were treated with different doses of DSG for 48 h. The mRNA levels of UHRF1 were analyzed by RT-PCR, β-actin was used as an internal control. The statistical significance was determined by student t-test, *** $p < 0.001$.

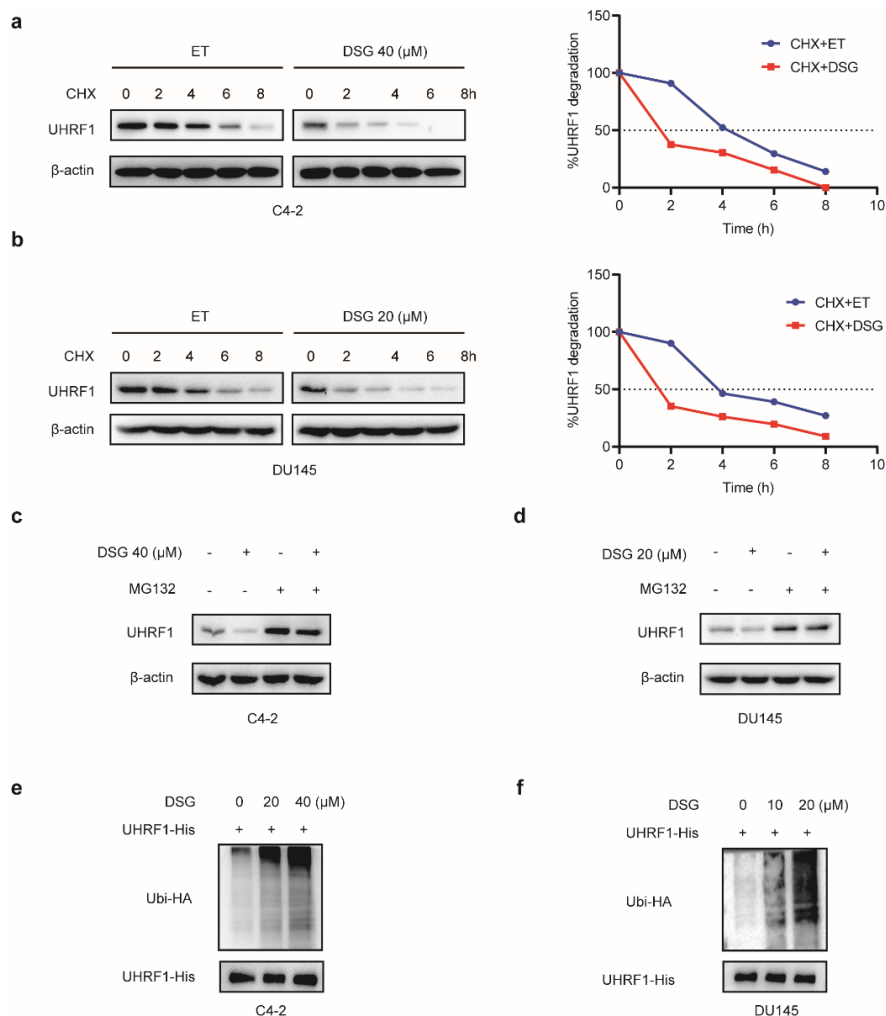


FIGURE 4. DSG induced UHRF1 protein degradation through the ubiquitin-proteasome system. **a-b** DU145 or C4-2 cells were treated with DSG for 40 h, and then treated with cycloheximide (CHX, 50 μg/mL). The proteins were harvested at the indicated time points, and UHRF1 levels were assessed by immunoblotting. β-actin was used as a loading control. The bands were quantified using densitometry analysis software. **c-d** Cells were treated with DSG for 42 h, followed by treatment with MG132(50 μM) for 6 h. UHRF1 protein was assessed by immunoblotting. **e-f** The plasmids expressing HA-ubiquitin and UHRF1-His were co-transfected to DU145 or C4-2 cells. The cells were treated with DSG at different doses for 48 h, and then followed by treatment with or without MG132(50 μM) for 6 h. UHRF1 was immunoprecipitated with anti-His antibody, and the polyubiquitylated UHRF1 was assessed with anti-HA antibody.

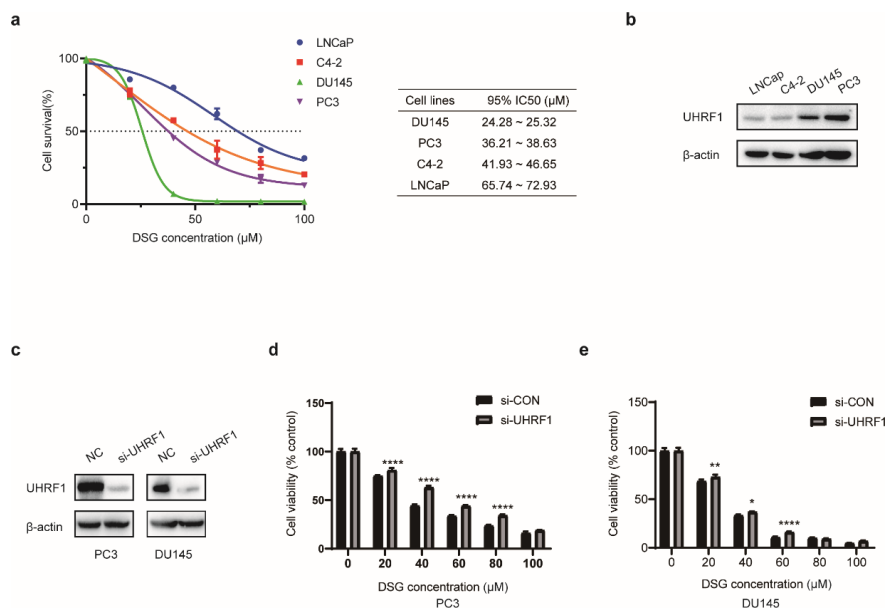


FIGURE 5. DSG inhibits cell survival by inducing UHRF1 protein degradation. **a** PCa cells were treated with different doses of DSG for 48h, and cell survival was analyzed by CCK8 assay. The IC50 values of DSG were calculated in different cell lines. **b** Protein levels of UHRF1 in different PCa cell lines were assessed by western blotting. **c** PCa cells were transfected with either scramble or UHRF1 siRNAs for 48 h. UHRF1 protein levels were assessed by western blotting. **d-e** UHRF1-knockdown DU145 and PC3 cells were treated with different doses of DSG for 48h, and cell survival were analyzed by CCK-8 assay. The error bars represent means \pm SDs, $n = 5$. Significance was determined by 2-way ANOVA and Tukey's method, * $p < 0.05$, ** $p < 0.01$, *** $p < 0.001$, and **** $p < 0.0001$.

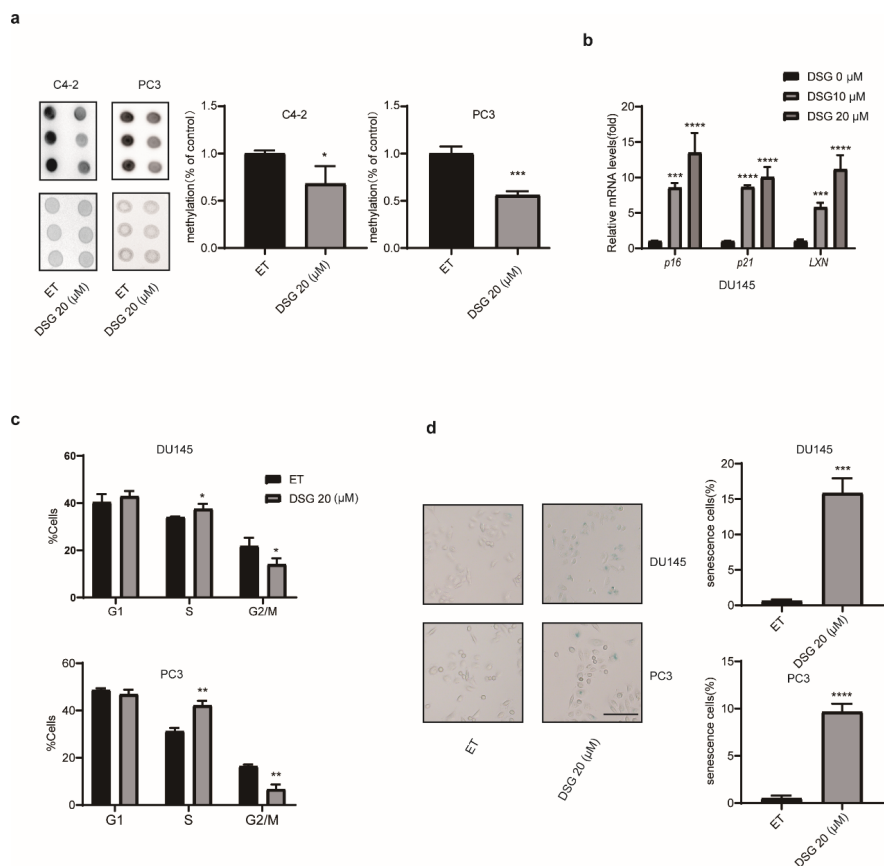


FIGURE 6. DSG reduced the genomic DNA methylation levels, and re-activated the expression of TSGs, resulting in cell cycle arrest and cellular senescence of PCa cells. **a** PCa cells were treated with DSG at different doses for 5 days, and then the genomic DNA was prepared. The levels of 5mC were assessed by DNA dot blotting, and the dot intensities were quantified. Significance was determined by Student's t-test, * $p < 0.05$; ** $p < 0.01$, *** $p < 0.001$. **b** DU145 cells were treated with DSG at different doses for 2 days, and the mRNA levels of TSGs were analyzed by RT-PCR, β -actin was used as an internal control. Significance was determined by one-way ANOVA and Tukey's method, * $p < 0.05$, ** $p < 0.01$, *** $p < 0.001$, and **** $p < 0.0001$. **c** DU145 or PC3 cells were treated with DSG for 3 days, and cell cycle was analyzed by cell cycle analysis kit. Significance was determined by Student's t-test, * $p < 0.05$, ** $p < 0.01$. **d** DU145 or PC3 cells were treated with DSG for 3 days and cell senescence was assessed by Senescence β -Galactosidase Staining assay. Scale bar indicates 100 μ m.

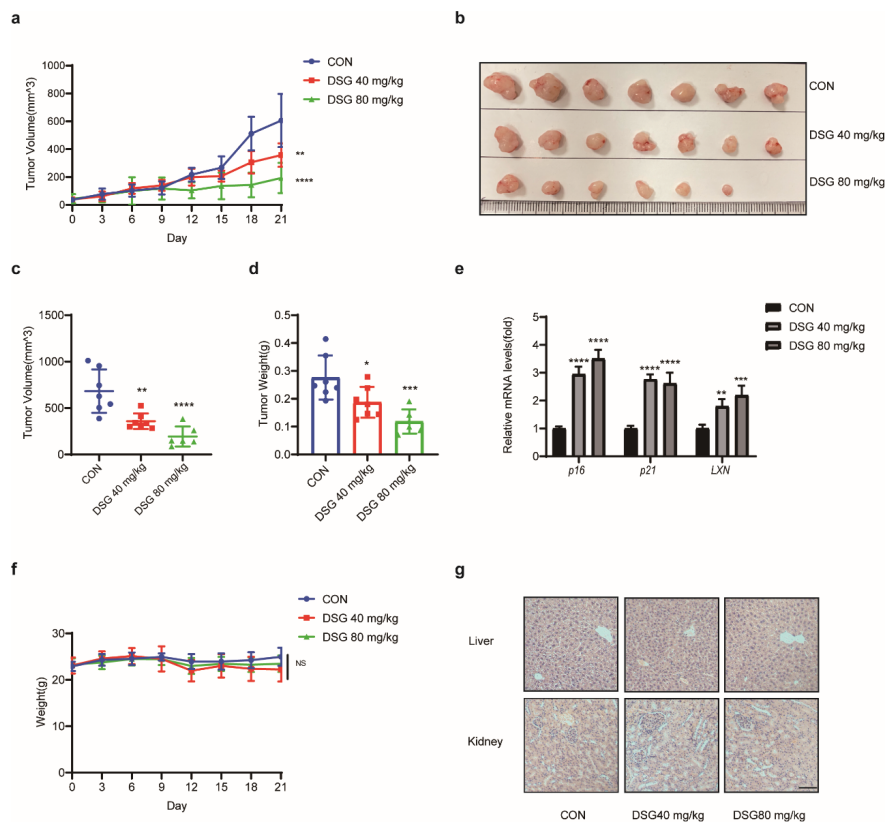


FIGURE 7. DSG inhibited the growth of PCa xenografts .a The growth curve of tumor xenografts were drawn when treated with different doses of DSG. **b** The dissected tumor nodes were compared at the endpoint of experiment. **c-d** Tumor volumes and weights of the dissected nodules. **e** The expression of typical TSGs inside tumors were analyzed by RT-PCR, β -actin was used as an internal control. **f** The body weight of nude mice was monitored throughout the whole duration of experiment. Significance was determined by one-way ANOVA and Tukey's methods, * $p < 0.05$, ** $p < 0.01$, *** $p < 0.001$, **** $p < 0.0001$. **g** Representative images of H&E staining of liver or kidney tissues. Scale bar indicates $100\mu\text{m}$.